Mineralogical Magazine, February 1998, Vol. 62(1), pp. 77–92

Hyalotekite, $(Ba,Pb,K)_4(Ca,Y)_2Si_8(B,Be)_2(Si,B)_2O_{28}F$, a tectosilicate related to scapolite: new structure refinement, phase transitions and a short-range ordered 3*b* superstructure

A. G. CHRISTY[1], E. S. GREW[2], S. C. MAYO[1], M. G. YATES[2] AND D. I. BELAKOVSKIY[3]

[1] Research School of Chemistry, Australian National University, GPO Box 414, Canberra, ACT 2601, Australia
[2] Department of Geological Sciences, 5711 Boardman Hall, University of Maine, Orono, Maine 04469-5711, USA
[3] A. E. Fersman Mineralogical Museum, Russian Academy of Sciences, Leninskiy Prospekt 18(2), Moscow 117071, Russia

ABSTRACT

Hyalotekite, a framework silicate of composition $(Ba,Pb,K)_4(Ca,Y)_2Si_8(B,Be)_2(Si,B)_2O_{28}F$, is found in relatively high-temperature ($\geqslant$ 500°C) Mn skarns at Långban, Sweden, and peralkaline pegmatites at Dara-i-Pioz, Tajikistan. A new paragenesis at Dara-i-Pioz is pegmatite consisting of the Ba borosilicates leucosphenite and tienshanite, as well as caesium kupletskite, aegirine, pyrochlore, microcline and quartz. Hyalotekite has been partially replaced by barylite and danburite. This hyalotekite contains 1.29–1.78 wt.% Y_2O_3, equivalent to 0.172–0.238 Y pfu or 8–11% Y on the Ca site; its Pb/(Pb+Ba) ratio ranges 0.36–0.44. Electron microprobe F contents of Långban and Dara-i-Pioz hyalotekite range 1.04–1.45 wt.%, consistent with full occupancy of the F site. A new refinement of the structure factor data used in the original structural determination of a Långban hyalotekite resulted in a structural formula, $(Pb_{1.96}Ba_{1.86}K_{0.18})Ca_2(B_{1.76}Be_{0.24})(Si_{1.56}B_{0.44})Si_8O_{28}F$, consistent with chemical data and all cations with positive-definite thermal parameters, although with a slight excess of positive charge (+57.14 as opposed to the ideal +57.00). An unusual feature of the hyalotekite framework is that 4 of 28 oxygens are non-bridging; by merging these 4 oxygens into two, the framework topology of scapolite is obtained. The triclinic symmetry of hyalotekite observed at room temperature is obtained from a hypothetical tetragonal parent structure via a sequence of displacive phase transitions. Some of these transitions are associated with cation ordering, either Pb–Ba ordering in the large cation sites, or B–Be and Si–B ordering on tetrahedral sites. Others are largely displacive but affect the coordination of the large cations (Pb, Ba, K, Ca). High-resolution electron microscopy suggests that the undulatory extinction characteristic of hyalotekite is due to a fine mosaic microstructure. This suggests that at least one of these transitions occurs in nature during cooling, and that it is first order with a large volume change. A diffuse superstructure observed by electron diffraction implies the existence of a further stage of short-range cation ordering which probably involves both (Pb,K)–Ba and (BeSi,BB)–BSi.

KEYWORDS: hyalotekite, scapolite, structure refinement, Långban, Sweden, Dara-i-Pioz, Tajikistan.

Introduction

HYALOTEKITE, $(Ba,Pb,K)_4(Ca,Y)_2Si_8(B,Be)_2(Si,B)_2O_{28}F$, is noteworthy for its eclectic chemical composition and extensive solid solution through the substitutions Pb $\rightleftharpoons$ Ba + K and 2B $\rightleftharpoons$ Si + Be (Moore *et al.*, 1982; Grew *et al.*, 1994). Only two occurrences are known: Mn skarns at the type locality of Långban, Sweden (Nordenskiöld, 1877; Lindström, 1887) and peralkaline pegmatites at Dara-i-Pioz, Tajikistan (Belakovskiy, 1991; Grew *et al.*, 1993, 1994). Moore *et al.* (1982) solved its crystal structure and emphasized the role of the lone-pair effect of Pb^{2+} in determining the splitting of Pb and Ba ions in the structure at room temperature. However, the Pb:Ba ratio of Moore *et al.* (1982), determined crystallographically, differed markedly from

those in the chemical analyses, and they reported a non-positive definite thermal parameter for a Pb site, features suggesting an imperfect modelling of the structure.

The presence of microcline-like undulatory extinction and incipient cross-hatch 'twinning' implied the possibility of phase transitions during cooling following crystallization and superstructures. Hyalotekite is inferred to be a relatively high-temperature mineral; Grew *et al.* (1994) estimated that it formed at $T \geqslant 500$°C. Moore *et al.* (1982) suggested that the lone-pair effect could be temperature dependent for Pb^{2+}, and hence that it would become operative only at low temperature.

In the present paper, we present new chemical and crystallographic data on hyalotekite from both Långban and Dara-*i*-Pioz, including a new refinement using the structure factors of Moore *et al.* (1982) , and an overall re-examination of its crystal structure.

Petrographic description

Two samples of hyalotekite are the subject of the present study, one each from the two known localities for this mineral: National Museum of Natural History, Smithsonian Institution, no. 114716 from Långban, and Hya-1 from Dara-i-Pioz. No. 114716 has been studied in considerable detail (Grew *et al.*, 1994), and another fragment from it was used for the structure refinement of Moore *et al.* (1982). The present paper reports the first description of Hya-1, which was collected in 1989.

No. 114716 consists largely of hyalotekite, quartz, aegirine, pectolite, calcite and hedyphane; melanotekite, barylite, andradite, hematite and baryte are minor (col. 1, Table 1, Grew *et al.*, 1994). At Långban, hyalotekite is an early formed mineral inferred to have formed at T = 500–600°C, $P \approx 2$–4 kbar (Grew *et al.*, 1994).

Principal constituents of Hya-1 are medium-grained (1–10 mm) caesium kupletskite [$(Cs,K,Na)_3(Mn,Fe^{2+})_7(Ti,Nb)_2Si_8O_{24}(O,OH,F)_7$], microcline, leucosphenite ($BaNa_4Ti_2(Si,B)_4Si_8O_{30}$) and hyalotekite, and finer grained aegirine, tienshanite [approximately $KBa_6Na_9Ca_2Mn_6(Ti,Nb)_6B_{12}Si_{36}O_{123}(OH)_2$], pyrochlore [$(Ca,Na)_2Nb_2O_6(OH,F)$] and quartz. Minor constituents are albite, polylithionite ($KLi_2AlSi_4O_{10}F_2$), barylite ($BaBe_2Si_2O_7$), danburite ($CaB_2Si_2O_8$), and an unidentified Ca-Ti-Pb phase. Hyalotekite forms grains roughly 2–4 mm across that show undulatory extinction. Some grains enclose rounded inclusions of tienshanite, and in places, hyalotekite and tienshanite are intergrown and appear to have crystallized coevally. Hyalotekite grains are partly surrounded by barylite in fine prisms and vermicular intergrowths with danburite. In places along hyalotekite grain margins, barylite and hyalotekite are intermixed on a micrometre scale resolvable only in secondary-electron images on the microprobe. These textures suggest partial breakdown of hyalotekite to barylite and danburite. Danburite also occurs interstitially to hyalotekite and leucosphenite or with tienshanite. Aegirine occurs with tienshanite and leucosphenite and fills fractures that appear to result from bending and breaking of the caesium kupletskite blades.

Hyalotekite paragenesis in Hya-1 differs markedly from that described by Grew *et al.* (1993, 1994) for hyalotekite in specimen 615/368 from Dara-i-Pioz. Both specimens are from Group III pegmatites, that is, pegmatites only found as loose blocks in moraine with no host rock attached (Belakovsky, 1991; Grew *et al.*, 1993). Specimen 615/368 belongs to the third type of Group III, reedmergnerite ($NaBSi_3O_8$)–microcline pegmatite, whereas specimen Hya-1 belongs to the second type, for which the principal constituents are feldspar, caesium kupletskite, tienshanite and hyalotekite (Belakovsky, 1991).

Grew *et al.* (1993, 1994) inferred two periods of crystallization for the reedmergnerite-bearing pegmatites and suggested that hyalotekite in specimen 615/368 crystallized during the later event by reaction of Pb- and Ba-bearing orthoclase with reedmergnerite and fluids containing Be. Hyalotekite in Hya-1 appears to have crystallized during the earlier event, presumably at T = 450–500°C and P $\leqslant$ 2 kbar, the conditions inferred for reedmergnerite crystallization (Grew *et al.*, 1993). During the later event, hyalotekite apparently broke down to barylite and danburite.

Chemical composition

Hyalotekite in both samples was analysed at the University of Maine using an ARL SEMQ electron microprobe equipped with Advanced Microbeam Micro-3WD automation. In the case of 114716, the same spots were analysed in this study as in the previous one (Grew *et al.*, 1994).

All elements were analysed using TAP, PET, and LiF wavelength-dispersive spectrometers (WDS) at 15 kV, 10 nA specimen current on quartz, an approximately 2 μm spot size, and 10 individual 10–30-second counts clustered within a 15 μm area. The standards were NBS K-456 Pb glass (70.14 wt.% PbO and 28.60 wt.% SiO_2) for Pb-*Mα*, periclase for Mg-*Kα*, wollastonite for Ca-*Kα* and Si-*Kα*, baryte for Ba-*Lα*, spessartine for Mn-*Kα*, orthoclase for K-*Kα*, jadeite for Na-*Kα*, $SrBaNb_4O_{10}$ for Sr-*Lα*, fluorite for F-*Kα*, $Y_3Al_5O_{12}$ for Y-*Lα* and hematite for Fe-*Kα*. The WDS counts were processed using $\phi(\rho z)$ matrix corrections (Scott and Love, 1992). which were applied not only to the measured constituents, but also to B and Be. Elements Si, Ca, K, Pb, Ba, Mg and Na (Hya-1, no. 4 only) were analysed using on-peak, mean atomic number background corrections, whereas Mn, Fe, F, Y, Sr, and Na (all other points) were analysed using peak-offset background corrections. We scanned Hya-1 for Ce, La, and Cs, but none of these elements were detected at the 0.1 wt.% level.

The new electron microprobe analyses of 114716 are in good agreement with those reported by Grew *et al.* (1994), although a different instrument, correction scheme, and, in some cases, different standards were used.

No new ion microprobe data were obtained in the present study. The B and Be data given in Table 1 for 114716 are from Grew *et al.* (1994), whereas those for Hya-1 were estimated as explained in the table notes.

Both samples are heterogeneous and vary in Pb, Ba and K from one grain to another. The compositions span most of the known range of Pb/(Pb + Ba) ratio: 0.36–0.52 (Table 1) *vs* 0.31–0.52 (Grew *et al.*, 1994). The relation between Ba + K and Pb in the new analyses for 114716 and Hya-1 is close to stoichiometric: Ba + K = 3.932 – 0.975Pb ($r^2 = 0.982$). Sample 114716 is also heterogeneous in B, Be and Si: its B/(B + Be + Si – 8) ratio ranges from 0.33 to 0.56 (this is the proportion of B calculated to be on the B and Si1 sites assuming that it is restricted to those sites: see below). The limited variation in Si in Hya-1 implies rather constant contents of B and Be in this sample.

Y is an important constituent of Hya-1 (analysis of the other Dara-i-Pioz sample, 615/368, gave about 0.4 wt.% Y_2O_3); low Ca contents in Hya-1 imply that Y substitutes for Ca on the Ca site.

F contents in both samples average close to one F per formula unit, which is consistent with the crystal structural refinement if no OH or O is incorporated on the F site (cf. ion probe values of 0.143–0.720 F and wet chemical value of 0.776 F pfu, Grew *et al.*, 1994). It is unlikely significant OH is present. G. R. Rossman (pers. comm., 1994) obtained about 120 ppm H_2O by infrared spectroscopy on a Långban hyalotekite (Swedish Museum of Natural History no. g29826, which is described by Grew *et al.*, 1994); this could be present as hydroxyl, equivalent to 0.02 OH per formula unit. Whether O is present on the F site cannot be resolved in a crystallographic refinement (see below).

New refinement of the hyalotekite structure

Some features of the refinement by Moore *et al.* (1982) indicate that the structure of hyalotekite was not completely modelled. In particular, the non positive-definite thermal parameter for Pb(1) is not physically realistic, and the refined Pb:Ba ratio of 29:71 is very low when compared to the 44:56–52:48 range obtained for Långban hyalotekites by probe or wet analysis (Grew *et al.*, 1994). A significant amount of K indicated by the analysis was not incorporated into the refinement, which may have affected both thermal parameters and occupancies on the large cation sites.

In order to investigate these problems with the refinement, we refined the structure again. The original structure factor data of Moore *et al.* (1982) was retrieved from microfiche archive, which unfortunately did not include sigma values. The data were converted to electronic form using a flat-bed scanner and character recognition software, and were extensively proof-read to correct mis-readings. The refinement was carried out on all 3713 independent reflexions using CRYSTALS (Watkin *et al.*, 1985). Refinement parameters are given in Table 2, atomic coordinates in Table 3, anisotropic displacement parameter data in Tables 4–5 (deposited with the Editor), and bonded and non-bonded interatomic distances in Tables 6*a*, 6*b* and 7 (Tables 6*b* and 7 are deposited with the Editor).

The structure of Moore *et al.* (1982) was used as a starting model for the refinement. Unit weights were used given the lack of sigma values. The occupancies of the (Pb, Ba) and (Si, Be) sites were constrained to total 1. The occupancies, along with anisotropic temperature factors and atomic coordinates were refined, giving a total of 237 parameters including the scale. In contrast to

TABLE 1. Analyses of hyalotekite and danburite

	114716-Cryst. 1982	Struct.* 1996	114716 1	114716 2	114716 3	114716 4	HYA-1 1	HYA-1 2	HYA-1 3	HYA-1 4	HYA-1 Danburite
Weight %											
SiO_2	39.19	38.01	37.76	40.66	39.41	39.69	38.43	37.91	37.36	37.69	49.62
FeO	–	–	0.00	0.02	0.01	0.01	0.01	0.01	0.02	0.01	0.00
MnO	–	–	0.19	0.08	0.15	0.24	0.05	0.19	0.02	0.09	50.02
MgO	–	–	0.00	0.00	0.00	0.00	0.00	0.00	0.00	0.00	0.00
CaO	7.61	7.42	7.54	7.63	7.47	7.42	6.52	6.42	6.41	6.44	22.53
K_2O	–	0.56	0.60	0.82	1.09	0.70	0.43	0.37	0.36	0.49	0.00
Na_2O	–	–	0.01	0.01	0.03	0.01	0.22	0.21	0.22	0.19	50.01
PbO	17.59	28.95	28.23	24.94	28.83	27.20	20.93	25.02	23.64	24.60	0.23
SrO	–	–	0.00	0.00	0.00	0.00	0.08	0.00	0.11	0.00	–
BaO	29.51	18.87	18.80	21.12	17.98	19.98	25.25	21.97	23.38	21.96	50.04
BeO#	0.64	0.40	0.28	0.96	0.33	0.83	0.25	0.25	0.25	0.25	–
B_2O_3#	4.72	5.07	5.05	3.03	4.56	3.93	5.30	5.30	5.30	5.30	28.60
Y_2O_3	–	–	0.07	0.21	0.11	0.27	1.74	1.29	1.74	1.78	–
F	1.29	1.26	1.24	1.45	1.32	1.19	1.16	1.24	1.28	1.04	–
F=O	−0.54	−0.53	−0.54	−0.61	−0.56	−0.50	−0.49	−0.52	−0.54	−0.44	–
Total	100.01	100.01	99.25	100.32	100.73	100.97	99.88	99.66	99.59	99.40	100.98

TABLE 1 (*contd.*)

	114716-Cryst. 1982	Struct.* 1996	114716 1	114716 2	114716 3	114716 4	HYA-1 1	HYA-1 2	HYA-1 3	HYA-1 4	HYA-1 Danburite
Formulae											
O	28.62	28.57	28.5	28.5	28.5	28.5	28.5	28.5	28.5	28.5	8
Si	9.62	9.56	9.530	10.040	9.752	9.791	9.469	9.477	9.390	9.436	2.010
Be#	0.38	0.24	0.170	0.569	0.196	0.492	0.148	0.150	0.151	0.150	–
B#	2.00	2.20	2.200	1.291	1.948	1.673	2.254	2.287	2.299	2.290	2.000
Fe	–	–	0.000	0.004	0.002	0.002	0.002	0.002	0.004	0.002	0.000
Sum IV	12.00	12.00	11.900	11.904	11.898	11.958	11.873	11.916	11.844	11.878	–
Mn	–	–	0.041	0.017	0.031	0.050	0.010	0.040	0.004	0.019	0.000
Ca	2.00	2.00	2.039	2.019	1.980	1.961	1.721	1.720	1.726	1.728	0.978
Na	–	–	0.005	0.005	0.014	0.005	0.105	0.102	0.107	0.092	0.000
Sr	–	–	0.000	0.000	0.000	0.000	0.011	0.000	0.016	0.000	–
Y	–	–	0.009	0.028	0.014	0.035	0.228	0.172	0.238	0.237	–
Sum	2.00	2.00	2.094	2.069	2.039	2.051	2.075	2.034	2.091	2.076	–
K	–	0.18	0.193	0.258	0.344	0.220	0.135	0.118	0.115	0.157	0.000
Ba	2.838	1.86	1.859	2.044	1.743	1.931	2.438	2.152	2.303	2.154	0.000
Pb	1.162	1.96	1.918	1.658	1.920	1.806	1.388	1.684	1.599	1.658	0.003
Sum	4.000	4.00	3.970	3.960	4.007	3.957	3.961	3.954	4.017	3.969	–
Total cations	18.000	18.00	17.964	17.932	17.946	17.967	17.910	17.903	17.953	17.924	4.990
F	1	1	0.990	1.132	1.033	0.928	0.904	0.980	1.017	0.823	–
Pb/(Pb + Ba)	0.29	0.51	0.51	0.45	0.52	0.48	0.36	0.44	0.41	0.43	–

Note: *Weight % were calculated from cation occupancies determined from crystal structure refinement by Moore *et al.* (1982) and this report (1996), for which the cation charges total +57.24 and +57.14, respectively.
#B_2O_3 and BeO. For 114716, values calculated from IMMA data reported by Grew *et al.* (1994) adjusted for the newly obtained SiO_2 contents. For HYA-1, values were estimated from SiO_2 and Si + Be = 11.939−1.014B and B = 19.547−1.817Si calculated from the new data on no. 114716 (cf. Grew *et al.*, 1994, Fig. 3). For danburite, B_2O_3 was calculated assuming ideal boron stoichiometry.

TABLE 2. Structure refinement parameters

Crystallographic data for hyalotekite:
Cell parameters: a = 11.310(2) Å, b = 10.955(2) Å, c = 10.317(3) Å α = 90.43(2)°, β = 90.02°, γ = 90.16° (Moore *et al.* 1982)
Space group: $I\bar{1}$ Cell content: $2[(Pb, Ba, K)_4Ca_2(B,Be)_2(Si,B)_2Si_8O_{28}F]$
Non-structural Data: No. of observed reflexions (from archive): 3713 Refinement method: full-matrix least-squares (CRYSTALS: Watkin *et al.*, 1985) Weighting scheme: unit weights (no σ values available). Number of parameters refined: 239 R factor: 0.061 Linear absorption coefficient (from refinement): 584 F (000): 1368.1 Density (calc): 3.953 g/cm^3 $\Delta\rho$ min/max: −2.8/+5.3*e*

the original refinement, the secondary extinction parameter was not refined.

Surprisingly, the refinement converged with significantly different Pb and Ba occupancies, giving a Pb:Ba ratio of approximately 40:60, and all thermal parameters positive definite. In a second stage of the refinement, potassium was included, sharing the barium sites. The positional and thermal parameters of K and Ba were constrained to be the same, and the total occupancy of the Pb+Ba+K split sites were held at approximately unity using restraints. Thus, the only additional parameters were the two K occupancies. The K(1) occupancy refined to a value smaller than the estimated error, so this was set to zero in subsequent refinement cycles. Although considerable correlation was observed between parameters, particularly occupancies and thermal parameters of site-sharing atoms, the refinement was well-behaved and converged normally. Final Pb:Ba:K ratios were 44:56:0 on the Pb/Ba(1) site and 54:37:9 on the Pb/Ba(2) site, giving an overall Pb:Ba:K of 98:93:9. The Pb:Ba ratio is well within the range expected from microprobe and wet analyses. The K total is just below the lowest value given in Table 1 for sample 114716, but accurate determination would not be expected for a minor low-Z substituent on a heavy atom site. The introduction of K was found not to be essential in order to obtain realistic thermal parameters but did improve the Ba:Pb ratio. We conclude that some aspect of the refinement strategy used by Moore *et al.* (1982) led them into a local minimum of R rather than the global minimum.

As in the original refinement, the Si:Be ratio on the Si(1) site refined to 81:19. However, the average Si(1)–O distance (1.597 Å) is short compared with those expected for Si–O (1.623–1.624 Å) or Be–O (1.634–1.637 Å) (Baur, 1981; Brown and Altermatt, 1985; Brise and O'Keeffe, 1991), which implies that at least some of the low-Z substituent on this site is actually B, not Be. The expected tetrahedral B–O distance is 1.477–1.478 Å. Refining the Si(1) site as (Si,B) gave a Si:B ratio of 78:22. It is not surprising that this is similar to the Si:Be ratio above, given the similar scattering factors for B and Be. The Si:B ratio estimated from bond lengths alone is very similar — 82:18.

Conversely, the bond length to oxygen for the 'B' site of hyalotekite is observed to be too long (1.495 Å) for occupation of this site by B alone. Attempts to introduce Si on this site in refinement cycles always led to its being rejected (i.e. the Si occupancy refined to zero). Be was too similar to B in scattering factor for its occupancy on the site to refine meaningfully, but the observed bond length is consistent with a B:Be ratio of 87:13 if the ideal bond lengths of Baur (1981) are used, or 89:11 for those of Brown and Altermatt (1985) and Brise and O'Keeffe (1991).

Only the average bond lengths can be used to estimate the occupancies of these sites given the

TABLE 3. Atomic coordinates and isotropic thermal parameters

Site	Occupancy*	x	y	z	U_{iso}**
Pb(1)	0.44(1)Pb	0.1577(3)	0.1742(2)	0.0049(1)	0.0110
Ba(1)	0.56(1)Ba	0.1947(5)	0.1970(4)	0.0123(2)	0.0169
Pb(2)	0.55(1)Pb	0.8370(5)	0.1764(3)	0.0056(1)	0.0164
Ba(2)	0.37(2)Ba				
	+0.09(1)K	0.7970(7)	0.2012(5)	0.0132(2)	0.0098
Ca		0.9997(1)	0.0030(1)	0.2287(1)	0.0096
B	B+Be	0.5001(8)	0.3365(8)	0.0303(8)	0.0106
Si(1)	0.78(2)Si				
	+0.22(2)B	0.3169(2)	0.5000(2)	0.9995(2)	0.0089
Si(2)		0.1938(2)	0.5266(2)	0.2483(2)	0.0086
Si(3)		0.8060(2)	0.5275(2)	0.2480(2)	0.0091
Si(4)		0.9995(2)	0.3222(2)	0.2629(2)	0.0101
Si(5)		0.0007(2)	0.7225(2)	0.2826(2)	0.0090
O(1)		0.8844(5)	0.6380(6)	0.3066(6)	0.0149
O(2)		0.8823(7)	0.4047(7)	0.2312(7)	0.0275
O(3)		0.1166(6)	0.4035(7)	0.2327(7)	0.0227
O(4)		0.1162(6)	0.6386(6)	0.3072(6)	0.0183
O(5)		0.2330(5)	0.5695(5)	0.1031(5)	0.0133
O(6)		0.7662(5)	0.5701(5)	0.1024(5)	0.0152
O(7)		0.6084(5)	0.4051(5)	0.0792(5)	0.0153
O(8)		0.3937(5)	0.4040(5)	0.0793(5)	0.0140
O(9)		0.5034(7)	0.2127(6)	0.0857(6)	0.0183
O(10)		0.4997(5)	0.6655(5)	0.1137(5)	0.0105
O(11)		0.0001(5)	0.7844(5)	0.1432(5)	0.0152
O(12)		0.9987(5)	0.2076(5)	0.1651(5)	0.0113
O(13)		0.3029(5)	0.5071(5)	0.3424(5)	0.0142
O(14)		0.6963(5)	0.5078(5)	0.3421(5)	0.0149
F	F(+O?)	0.0000	0.0000	0.0000	0.0194

* this column blank if site fully occupied by atom specified in the label
**geometric mean of principal axes of thermal ellipsoid

TABLE 6*a*. Bond lengths for tetrahedral cations (Å)

B–O(9)	1.476(10)	Si(1)–O(7)	1.569(7)
B–O(10)	1.485(10)	Si(1)–O(8)	1.599(6)
B–O(8)	1.500(11)	Si(1)–O(6)	1.601(6)
B–O(7)	1.520(1)	Si(1)–O(5)	1.617(6)
mean	1.495	mean	1.597
Si(2)–O(13)	1.585(6)	Si(3)–O(14)	1.591(6)
Si(2)–O(3)	1.611(7)	Si(3)–O(2)	1.609(7)
Si(2)–O(4)	1.624(6)	Si(3)–O(1)	1.613(6)
Si(2)–O(5)	1.634(6)	Si(3)–O(6)	1.639(6)
mean	1.614	mean	1.613
Si(4)–O(12)	1.605(6)	Si(5)–O(11)	1.595(6)
Si(4)–O(9)	1.612(6)	Si(5)–O(4)	1.621(6)
Si(4)–O(3)	1.626(7)	Si(5)–O(10)	1.622(6)
Si(4)–O(2)	1.640(7)	Si(5)–O(1)	1.626(6)
mean	1.621	mean	1.616

similar, small scattering factors of B and Be. However, both overall scattering factors for the Si(1) and B sites and the bond lengths are explained if the substitution pattern on these sites is actually $(B_{1-x}Be_x)(Si_{1-y}B_y)$ rather than $B(Si_{1-y}Be_y)$. This substitution seems reasonable given that the size and electronegativity differences between Be and B are comparable to those between Al and Si, or Mg and Fe. Substitution between B and Be is also found in rhodizite, $(K,Cs,Rb,Na)Al_4Be_4(B,Be,Li)_{12}O_{38}$ (Pring *et al.*, 1986). Short-range order on these sites may well be involved in formation of a diffuse superstructure observed in TEM (see below).

No attempt was made to refine the F:O ratio on the F site, since these atoms again scatter very similarly.

Overall, most structural features in our refinement are very similar to those in Moore *et al.* (1982). Heavy atom occupancies are discussed above. In general, the shortest bonds to M = {Ba, Pb, K, Ca} are longer in our refinement, and the longest bonds shorter, giving more regular coordination polyhedra around the large cations. No M–O distance that we assume to be bonded is longer than a M–M distance (Moore *et al.* give Pb(1)–O(3) = 3.470 Å and Pb(1)–Ca = 3.441 Å). Conversely, all M–O distances that are less than any cation–cation distance are assumed to be bonded. This cut-off distance is 3.47 Å for (Pb, Ba, K) in our refinement. It is interesting to note that the shortest M–M distances are very close to the 3.50 Å nearest-neighbour distance of Pb metal, as in $(Pb_2O)(Pb,K)_4Si_8O_{20}$ (Moore *et al.* 1985). The shortest Ca–Si distances are similar, whereas one Ca–B distance is much shorter (3.03 Å). This short non-bonded distance arises because of the deviation of the unit cell from orthorhombic symmetry, and concomitant rotation of the $(Si,B,Be)_4O_{12}$ rings out of the (001) plane. Presumably, it is permissible because B has a much smaller non-bonded radius than Si (1.23Å as opposed to 1.53 Å: O'Keeffe and Hyde, 1981).

The Ba–F distances are increased considerably in our refinement. Interestingly, the Ba(2)–O(9) distance is concomitantly shortened so as to increase the coordination number of Ba(2) from 9 to 10. The increase in size and coordination number of Ba(2) relative to Ba(1) may account for the preferential accommodation of K on this site. The increase in coordination number of the Ba(2) site provides a topological rationale for the shear that reduces the symmetry of hyalotekite from monoclinic to triclinic.

Bond lengths in the tetrahedral framework were in close agreement with the original refinement. As in Moore *et al.* (1982), the bonds from Si to the non-bridging oxygens are *ca.* 0.02 Å shorter than to bridging oxygens, as expected. In general, the vibration ellipsoids in our refinement are more anisotropic than their counterparts in Moore *et al.* (1982). In particular, the ellipsoids for O(2), O(3) and O(9) all have a very long major axis. This may indicate some additional substitutional or positional disorder which is not taken into account in our model structure. It is evocative to note that all three of these oxygens are bonded to Si(4), and that O(9) is bonded to the B site also. Both of these tetrahedral sites show somewhat longer mean bond lengths to oxygen than expected, which may also be related to disorder.

The formula, based on our refinement, is:

$$(Pb_{1.96}Ba_{1.86}K_{0.18})\ Ca_2(B_{2-x}Be_x)(Si_{1.56}B_{0.44})Si_8O_{28}F$$

The Be content x is not known from the refinement but should be 0.38 for overall electroneutrality (less if there is oxygen on the F site), or can be estimated as 0.22–0.26 from the average bond length for the B site. These estimates compare well with the analyses of Table 1 (note particularly column 3).

At the end of the refinement, a Fourier difference map was calculated to examine the remaining electron density. No significant excess peaks or troughs were observed on the atoms themselves, the largest residua on sites being $+0.3e$ on Pb(2) and $-0.4e$ on Si(4). However, significant deviations did occur elsewhere. The lowest minimum observed was $-2.8e$. The most positive features were two peaks of $5e$ and $3e$ that lay in the same [xy0] plane as the (Pb, Ba, K) sites, close to the Pb(2) positions. The larger peak lies 1 Å from Pb(2) and about 1.8 Å from O(11) and O(12); the smaller peak is 1 Å from Pb(2) on the other side. These peaks are in one-sided pyramidal coordination environments compatible with their being alternative Pb(2) positions of extremely low occupancy (3–6%). A much higher occupancy would be required if light elements provided this electron density. Such high occupancy would be incompatible with a high occupancy for Pb(2) given that the sites are too close for simultaneous filling. Alternatively, these peaks arise from inadequate modelling of the Pb electron distribution. Coordinates and bond lengths for these maxima are assumed to be of low accuracy and are not included in Tables 3–7.

Structure description

The incompletely connected tetrahedral framework of hyalotekite is described in detail in Moore *et al.* (1982). The framework contains 4- and 8-rings of tetrahedra, reminiscent of the feldspar structure, but linked very differently. The hyalotekite structure incorporates a corrugated T_4O_{10} layer parallel to (001) which is similar to that of gillespite ($BaFeSi_4O_{10}$).

An unusual feature of the hyalotekite framework is that 4 out of 28 oxygens are nonbridging, giving an overall framework stoichiometry of $T_{12}O_{28}$ rather than $T_{12}O_{24}$. Perhaps the most significant relationship to another structure is seen if these oxygens are merged pairwise so that the framework is fully 4-connected. The atoms in question are the O(11)–O(12) and O(13)–O(14) oxygen pairs according to the numbering scheme of Moore *et al.* (1982). The members of each of these pairs approach each other closely along **c**. If the pairs are replaced by single oxygens which link pairs of tetrahedral cations: Si(4)– O(11/12)–Si(5′) and Si(2)–O(13/14)–Si(3′), the topology of the scapolite framework is obtained (Fig. 1). It is noteworthy that the zeolite maricopaite has a framework derived from that of mordenite by a similar breakage of links between tetrahedra (Rouse and Peacor, 1994). Interruption of the framework causes opening of pairs of 5-rings in scapolite to become 8-rings in hyalotekite (Fig. 1), and also opens combinations of two 5-rings and an 8-ring, roughly parallel to {110}, to open into a cruciform 14-ring. Similarly, pairs of 4-rings and an 8-ring in mordenite open into a cruciform 12-ring in maricopaite (Rouse and Peacor, 1994). In both hyalotekite and maricopaite, interruption of the framework is associated with the presence of lead in the channels of the structure. The lead forms polynuclear clusters with the nonbridging oxygens: $Pb_4(O,OH)_4$ units in maricopaite and $Ca_2Pb_4O_8F$ in hyalotekite. The Pb–O bonds within these clusters are appreciably shorter than the bonds to bridging oxygens. For hyalotekite, the ranges are 2.35–2.59 Å to non-bridging oxygen and fluorine, and 3.15–3.47 Å, to the other 3 oxygens in the Pb coordination polyhedron. The shapes of the clusters can be described as a tetrahedron of oxygens with Pb outside the face centres (maricopaite), and as a cube of oxygens with Pb outside four of the faces, F at the centre of the cube and two Ca capping the remaining cube faces (hyalotekite). In both cases, interruption of the framework of a more familiar structure appears to be driven by the tendency of Pb to show a stereochemically active lone pair, and hence adopt an asymmetric coordination environment in which a few bonds on one side of the cation (Pb–F and 4 Pb–O in hyalotekite) are shorter and stronger than the rest. It is possible, as Rouse and Peacor suggest, that the Pb existed as such clusters in the aqueous solutions from which the minerals crystallized.

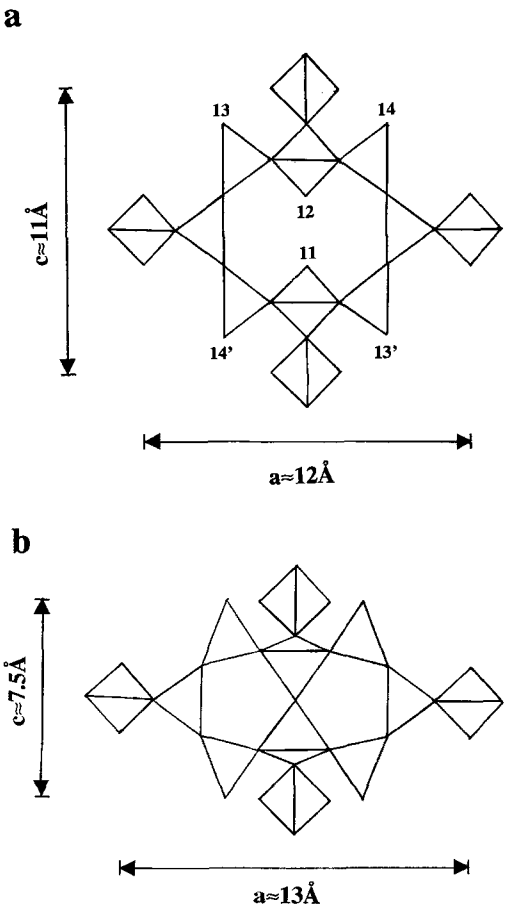

FIG. 1. Comparison of portions of (*a*) the hyalotekite framework and (*b*) corresponding portion of the scapolite structure. Both structures are idealized and have their maximum possible *I4/mmm* symmetry. Nonbridging oxygens in (*a*) are numbered according to the scheme of Moore *et al.* (1982).

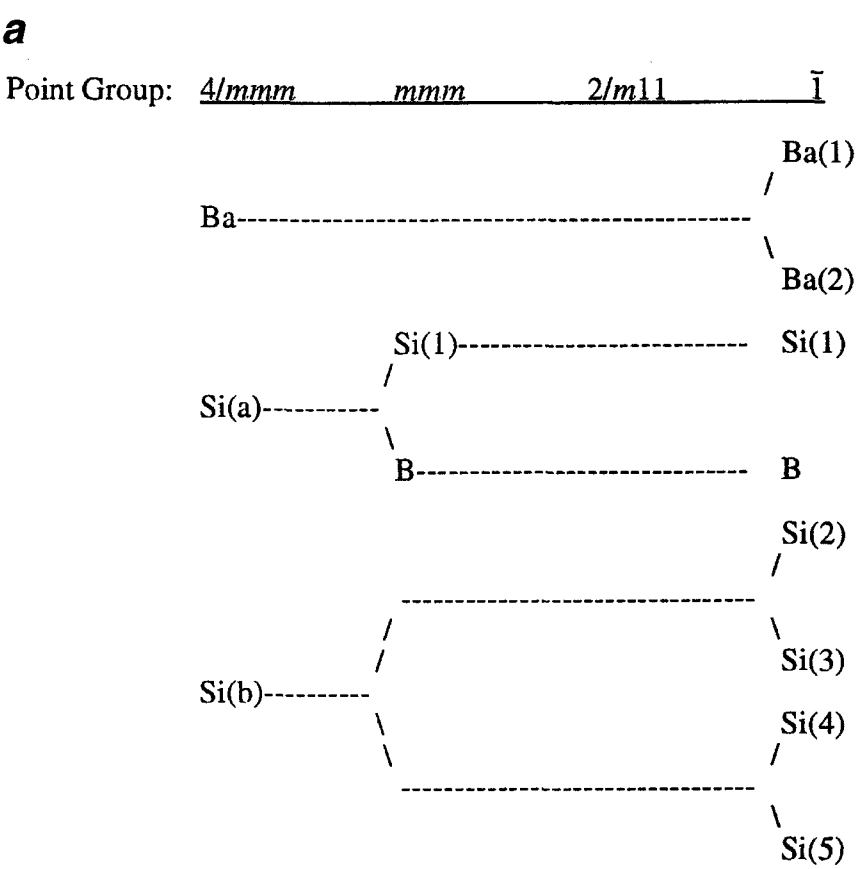

FIG. 2. Splitting of hyalotekite atom sites as the symmetry is lowered stepwise from *I*4/*mmm* to *I*1̄. (*a*) cations, (*b*) (opposite) anions. Note: Pb site splits in a similar fashion to the Ba site. The Ca and F sites do not split.

Large-cation clusters topologically identical to those of hyalotekite are also found in the synthetic compound $(Pb_2O)(Pb,K)_4Si_8O_{20}$ (Moore *et al.*, 1985). The silicate anion in this compound is a tubular *vierer* double chain aligned along a 4_2 screw axis, similar to that in narsarsukite, $Na_4Ti_2O_2Si_8O_{20}$ (Peacor and Buerger, 1962). In the lead potassium silicate, these chains are cross linked by octahedral clusters $Pb_2(Pb,K)_4O_8O$ which, again, are topologically the same as the $Ca_2(Pb,Ba,K)_4O_8F$ groups in hyalotekite. As in hyalotekite, the Pb and K atoms occupy split sites, with centroids 0.59 Å apart (Moore *et al.*, 1985). A lead-free, incomplete cluster $\square_2Ca_4O_8F$ cross-links the silicate layers of the mineral apophyllite, $KCa_4Si_8O_{20}F{\cdot}8H_2O$ (Taylor and Náray-Szábo, 1931). In the apophyllite cluster, the Ca atoms are in positions corresponding to those of (Pb,Ba,K) in hyalotekite.

Potential for structural phase transitions

The maximum possible space group symmetry for a framework of scapolite or hyalotekite topology is *I*4/*mmm*. However, the observed symmetry is much lower than tetragonal but closely approximates *I*2/*m*11 (the pseudodiad is parallel to the **a** axis). A particular sequence of discrete *zellengleich* structural distortions, preserving the unit cell content, needs to operate so as to reduce the symmetry to triclinic. Each of these elementary steps of the sequence has the symmetry properties of an irreducible representation of a higher symmetry phase, and reduces the symmetry of

b

Point Group: 4/*mmm* *mmm* 2/*m*11 Ī

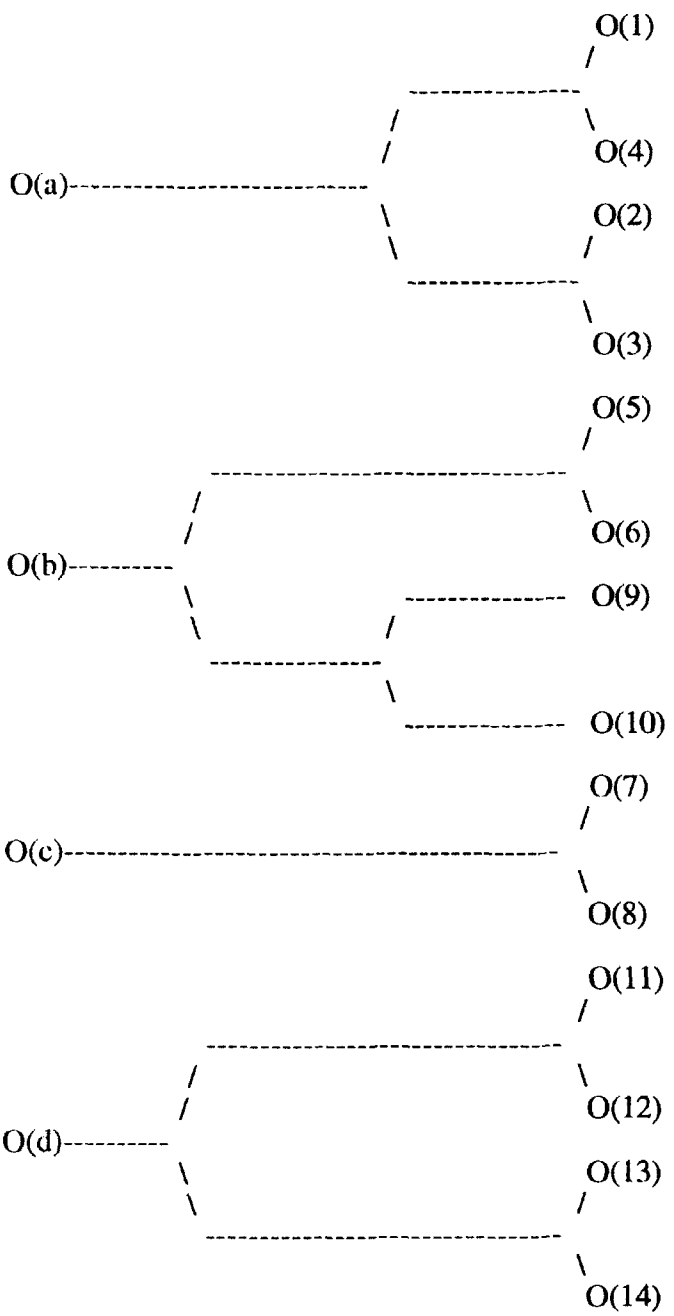

that structure to that of the next in the sequence. Any of these steps *could* occur as continuous (second-order) transition; alternatively, a first-order transition may take the structure through one or more such steps at once. Consideration of group–subgroup relationships allows the steps to be enumerated. Each step may involve ordering, atomic displacements or both, depending on how the atomic site symmetries are affected. The operation of these symmetry-reducing processes may be reflected in the occurrence of phase transitions between states of different symmetry at elevated pressure or temperature, although no such transitions have been reported for hyalotekite to date. The symmetry-reducing steps are called 'transitions' below in the light of this possibility. The steps from tetragonal to triclinic symmetry are as follows.

(i) An order–disorder transition transforming as the B_{1g} representation of *I*4/*mmm* may reduce the symmetry to orthorhombic *Immm*. Such a transition would split the B and Si(1) sites of hyalotekite, thus distinguishing the (B,Be) and (Si,B) sites. The Si atoms in the other four rings, which are all equivalent in *I*4/*mmm*, also split into two pairs, Si(2/3) and Si(4/5). Two oxygen sites split also (Fig. 2).

(ii) *I*2/*m* symmetry may be attained either from *Immm* with the A_{1g} representation active, or directly from *I*4/*mmm* according to the doubly degenerate E_g representation. No cation sites are split further by this symmetry reduction, but some oxygen sites of the orthorhombic and tetragonal phases are split into pairs (Fig. 2). This transition would be displacive in character, allowing no further cation ordering. However, the loss of orthorhombic symmetry allows tilting of the Si(1)–B 4-rings out of the (001) plane, as noted earlier. This tilting is very apparent in the structure diagram of Moore *et al.* (1982). The rotation moves one O(7) and one O(8) out of the Ca coordination polyhedron and brings an O(10) into it, giving the 8-fold coordination of Ca seen in the structure as refined.

(iii) Si(2/3) and Si(4/5) are further split by a symmetry reduction to $I\bar{1}$ according to the B_g representation of *I*2/*m*. All oxygen sites except two split, as do the (Ba,Pb) sites (Fig. 2). All the sites Si(2)–Si(5)are fully occupied by Si, and a difference in occupancy and coordination for the two large cation sites is now permitted by symmetry. Therefore, there may be both order–disorder and displacive character to this transition. The different Ba:Pb:K ratios of the sites and coordination numbers in our refinement imply that both occur. Since Pb(1) and Ba(1) are separated along a vector close to [110] whereas the Pb(2)–Ba(2) vector is near $[1\bar{1}0]$, the *xy* (e_4) strains associated with partitioning Pb into Pb(1) and Pb(2) have opposite signs, and differential occupation of these sites may be important in causing the symmetry drop from monoclinic to triclinic.

None of the transitions hypothesized above determine whether the Pb and (Ba,K) sites split. This is because the symmetry of these sites in the tetragonal structure (Wyckoff site 8*h*, 2*mm* point symmetry) is sufficiently low for Pb and Ba centroids to be split even in the tetragonal phase. Therefore, any transition from a structure in which Pb is on the same sites as the other large cations is isosymmetric (Christy, 1995). Merging of the Pb and (Ba,K) sites at high temperature was postulated by Moore *et al.* (1982) in order to explain the extensive solid solution of Pb and Ba despite their different stereochemistries at room temperature. Splitting or merging of the sites may occur in tetragonal, orthorhombic, monoclinic or triclinic variants of the hyalotekite structure without symmetry change. Only the symmetry of the Pb–Ba vector changes with crystal system. In *I*4/*mmm*, Pb and Ba may separate along the <110> diad on which they lie. In *Immm*, an extra degree of freedom is gained since the displacement is unconstrained in the *xy* plane, and in *I*2/*m* a *z* component to the displacement is allowed. The refinement shows that the *x* and *y* components of the ~0.5 Å site splitting are comparable in magnitude but distinctly different and that the *z* component although smaller, is non-zero, implying that distortion away from tetragonal symmetry may have facilitated an increase in the Pb–(Ba,K) distance to its observed value even though symmetry reduction is not essential for non-zero site splitting. The symmetric constraints on Pb lone pair orientation in the orthorhombic and tetragonal structures may lead to the asymmetric Pb atom acting as a brace, increasing the volume and lowering the compressibility of the higher-symmetry structures. Similar behaviour has been noted for the linear hydrogen fluoride ion in rhombohedral $NaHF_2$ (Christy *et al.*, 1992). This would tend to destabilize the high-symmetry structures under high-*P* and/or low-*T* conditions, and is consistent with the fact that these higher-symmetry variants of the hyalotekite structure have not been observed to date.

Grew *et al.* (1994) noted that Långban hyalotekite in thin section shows "undulatory extinction and locally has a patchy extinction suggestive of incipient cross-hatch twinning reminiscent of microcline". The other hyalotekite examined in this study (from Dara-i-Pioz, Tajikistan) also shows undulatory extinction in optical microscopy. The optical inhomogeneity may be due to the presence of micron-scale twinning which may have occurred at a phase transition from higher symmetry. The analysis of the hyalotekite structure presented above shows that this supposition is very reasonable, since the triclinic structure observed under ambient conditions can be derived from monoclinic and orthorhombic variants by displacive transitions alone, and from a tetragonal phase by ordering of (B,Be) and (Si,B). Because the texture was too fine to be resolved by optical microscopy, it was decided to examine hyalotekite microstructure by transmission electron microscopy.

Electron microscopy

Experimental

Grains of sample 114716 (Långban) and Hya-1 (Dara-i-Pioz) were prepared for the electron microscope by three different methods.

(*i*) Fragments were crushed and then sedimented onto copper mesh grids from ethanol.

(*ii*) Hyalotekite has distinct cleavages which may give rise to prefered orientations for crystal settling if method (*i*) is used. Planar defects parallel to the cleavage planes would tend not to be observed. Therefore, some crushed grains were pressed into disks of indium foil, and the foil then thinned with an argon ion beam, so as to obtain a less biassed selection of crushed grain orientations.

(*iii*) If planar features such as antiphase domain and twin boundaries are separated by average distances greater than the grain size (~0.1 μm), they will be observed with disproportionate rarity. Therefore, cleavage flakes of hyalotekite, about 2 mm in diameter, were attached to copper foils and beam thinned, providing tens of microns of continuous thinned edge for examination.

All specimens were examined in a Philips EM430 microscope operating at an accelerating voltage of 300 kV. The specimen holder allowed tilt of $\pm 70^\circ$ about two orthogonal axes. The combination of this wide range of tilt with the three different specimen preparation methods described above renders it unlikely that any pervasive microstructures would have been overlooked.

Results

Both samples contained abundant low-angle grain boundaries. These are likely to be the cause of the uneven extinction in optical microscopy. No twin boundaries were seen. Electron diffraction patterns showed some streaking, which was recorded in a variety of orientations. It should be noted that the closeness to 90° of the hyalotekite α, β and γ angles resulted in all patterns being apparently orthorhombic. Therefore, there is an ambiguity of parity for most Miller indices. **a***, **b*** and **c*** were distinguishable by careful comparison of reflection spacings even though the reciprocal lattice repeats are all within ±10% of each other. In the discussion below, internal consistency has been maintained, but it is possible that the *k* and *l* indices should have their signs relative to *h* reversed.

Examination of the negative of a $[10\bar{1}]$ diffraction pattern from Långban hyalotekite revealed that continuous streaks were present parallel to **b***, and passed through the Bragg reflections (Fig. 3*a*). Diffuse maxima were present on the streaks at approximately $\pm\mathbf{b}^*/3$ relative to the Bragg peaks. A $[\bar{1}31]$ pattern from the Dara-i-Pioz sample showed faint streaks parallel to $(310)^*$ and $(01\bar{3})^*$ (Fig. 3*b*), which showed maxima at positions consistent with those of Fig. 3*a*. The occurrence of the diffuse maxima in both samples implies that both had a similar short-range ordered 3*b* superstructure. The differing directions of the streaks may imply that domains were lamellar on (010) in the Långban sample, but lamellar on {310} and $\{01\bar{3}\}$ in that from Dara-i-Pioz. It is also possible that both sets of streaks were present in the diffraction patterns of both samples, but grain orientations showing both sets were not observed. Very faint streaks parallel to two $(110)^*$ or $(011)^*$-type directions were also observed in one Dara-i-Pioz diffraction pattern taken down a <111>-type axis, but no diffuse maxima were associated with these. A similar set of faint streaks was observed parallel to $(110)^*$ or $(011)^*$ in a pattern taken with the beam nearly parallel to $[\bar{1}10]$ or $[01\bar{1}]$ respectively. No diffuse structure was seen in Långban [010] images (Fig. 3*c*) . It appears that all streaks have a component along **b***. Attempts to image the domain structure under dark-field conditions and in high resolution mode were unsuccessful. In the latter case, very uniform lattice images of the sublattice were obtained. It

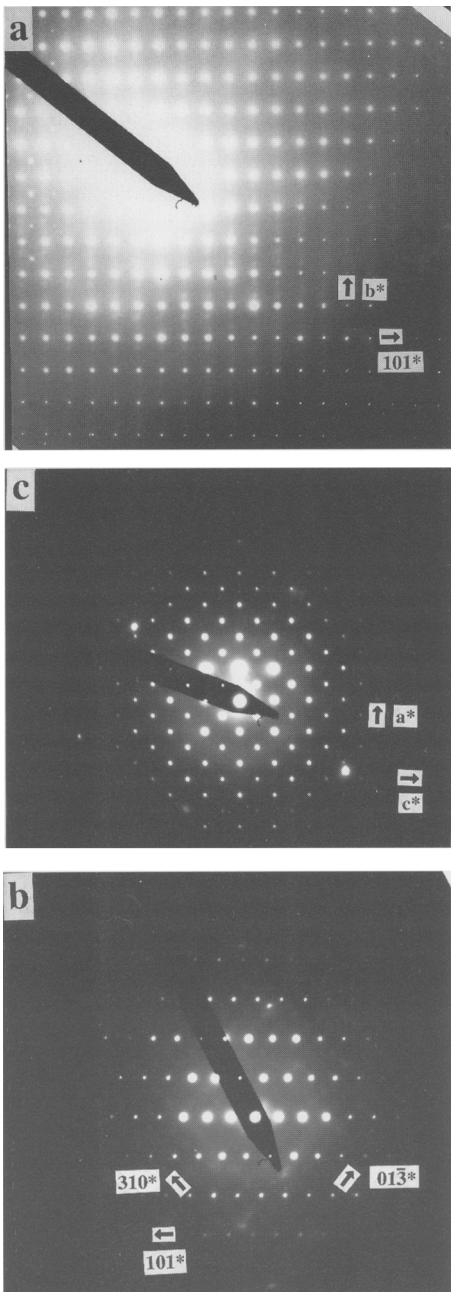

FIG. 3. (*a*) Electron diffraction pattern with beam parallel to [10$\bar{1}$]. Overexposed near origin to show up the diffuse streaks. Långban sample. (*b*) Diffraction pattern with beam parallel to [$\bar{1}$31]. Dara-i-Pioz sample. (*c*) Diffraction pattern with beam parallel to [010]. Långban sample. Camera length was 1200 mm for all diffraction patterns.

appears that the domain structure produces very little contrast.

Discussion

The mosaic structure

The subgrain boundaries in both hyalotekite specimens imply that the samples have undergone annealing and partial recovery after being strained. The presence of similar mosaic microstructures in specimens from two radically different geologic environments (skarn at Långban, pegmatite at Dara-i-Pioz) suggests that the microstructures resulted from a phase transition rather than externally applied stresses. In both cases, hyalotekite crystallized at $T \geqslant 500°C$ and was subsequently affected by an event at lower temperature. Growth in the *I*4/*mmm* phase would require complete disorder of Be, B and Si on the Si(a) sites (Fig. 2*a*). This seems unlikely, so the original symmetry was probably not higher than orthorhombic. Maintenance of the observed Ca coordination topology would restrict it to monoclinic. At least one transition involved a sufficiently large volume change for the overall coherence of the lattice to be partially lost, giving rise to the observed subgrain boundaries. The loss of lattice integrity suggests that the spontaneous strain arising from the transition was large compared to that for displacive transitions in other framework silicates such as the silica polymorphs, feldspars and feldspathoids. It also suggests that the transition was thermodynamically first order, with a discontinuity in volume. Orientational ordering of the lone pair on the Pb may be sufficient to drive a strong contraction of the structure, and loss of bracing function upon gaining a new degree of orientational freedom may do likewise. A transition from dynamic disorder to static order in the orientation of SH groups in NaSH causes a 13% volume decrease at a few kilobars pressure (Haines and Christy, 1992), and rotation of the anions in $NaHF_2$ causes a collapse of similar magnitude (Christy *et al.*, 1992). Similarly, re-ordering of an effectively non-spherical Pb may well be associated with a marked framework collapse and symmetry change.

The 3b superstructure

An important feature of the crystal chemistry of hyalotekite is that solid solution is necessary to maintain electroneutrality. The dominant cations

on each site, $[Pb_2Ba_2Ca_2B_2Si_2Si_8]$, have a total charge of +58, as opposed to −57 for the anions $[O_{28}F]$.

The total positive charge is reduced to a small degree by substitution of K for Ba(2), and more significantly by Be replacing B and B replacing Si(1). All of these substitutions, and additional Pb replacing Ba and Y replacing Ca, will have their effect on local charge balance. It is likely that interaction between them is responsible for the observed diffuse modulation. We consider first the possibility that the superstructure is caused by further ordering of Be, B and Si. Note that in the substitutional scheme that fits the structure refinement best, the minority constituents on both the B site and the Si(1) site have lower valences than the majority constituent. The presence of both Be substituting for B and B for Si(1) in the same 4-ring would therefore cause an appreciable local charge imbalance. Furthermore, although the total lengths of (B−O)+(Si−O) and (Be−O)+(B−O) are similar, the relative lengths of the two bonds are reversed in the latter pair. This suggests that simultaneous substitution would displace O(8) by about 0.16 Å towards Si(1). The thermal parameters for O(8) are not especially large or anisotropic (Tables 3−4), which suggests that the two substitutions do not occur together. Therefore, it seems likely that there are three principal types of B−Si(1) 4-rings: $B_2Si_2O_{12}$ (the majority), $(B,Be)_2Si_2O_{12}$ (lower mean cation valence, larger mean bond lengths) and $B_2(Si,B)_2O_{12}$ (lower valence, smaller bond lengths). The total percentage of the low-valence rings is constrained by the need to maintain overall charge balance. For the analyses of Table 1, the sum of Be and $B_{Si(1)}$ is 0.43−0.68, so this percentage is 21−34% assuming one minority substituent per ring. The proportions of Be- and B-rich rings vary widely: the analysis of Table 1, column 4, indicates 0.57 Be per formula unit but no excess B (−0.14 B on the Si(1) site pfu) whereas columns 8−10 show about 0.15 Be pfu and 0.45 B on Si(1). Charge imbalance and lattice strains would be minimised if low-valent rings were kept as far separate from each other as possible. This is a likely cause of superstructure development.

Ba and Pb are also very likely to order in hyalotekite. One driving force for this process would be the off-centring of Pb atoms relative to the Ba sites, which would couple strongly to the deformation of the immediately surrounding berylloborosilicate framework. The less symmetrical bonding around Pb as compared with Ba, and the low valence of K, cause underbonding on oxygens O(5)−O(10). This would exacerbate the underbonding of these oxygens due to an adjacent 4-ring of low valence. Conversely, Y substitution for Ca increases bond strength to O(7), O(8), O(10) and O(11), and hence compensates for the effect of low-valent 4-rings or (Pb,K). The need to maintain local charge balance implies that avoidance would be likely between low-valent 4-rings and (Pb, K). The observed range of ratios (Pb+K)/(Pb+Ba+K) is 0.38−0.57 (Table 1). Since the proportion of (Pb,K) is less than 2/3, and the proportion of low-valent 4-rings is 1/3 or less, it would indeed be possible to minimise close juxtapositions of the two by ordering them in antiphase in a threefold superstructure such as that observed in TEM. The extra diffraction spots remain diffuse because the coherence length of the ordering is short, and domains are probably only a few supercells across. This is consistent with the superstructure being a product of ordering at low temperature, where diffusion distances are short.

Conclusions

Hyalotekite is shown to be a partially depolymerized, cation-ordered and displacively distorted relative of the scapolite group of minerals. The cluster of anions and large cations that replaces scapolite bridging oxygens also occurs in the $(Pb_2O)(Pb,K)_4Si_8O_{20}$ structure and in an incomplete form in apophyllite. New compositional data reveal the possibility of substantial Y substituting for Ca in hyalotekite, and a new refinement gives improved thermal parameters for all atoms and Ba:Pb:K ratios on the large 9−10 coordinated cation sites. A mosaic microstructure permeating samples from two different geological environments suggests that triclinic hyalotekite in both localities may have gone through at least one of the possible phase transitions that relate it to a hypothetical tetragonal aristotype. TEM examination also shows the existence of diffuse diffraction maxima from an incipient cell-tripling superstructure along **b***. The short-range ordering responsible for this superstructure is likely to involve a combination of both ordering of (Pb,K) *vs* Ba, and of (BeSi, BB) versus (BSi).

Acknowledgements

We would like to thank the National Museum of Natural History (Smithsonian Institution) for the

provision of sample 114716, and the Swedish Museum of Natural History for sample g29826. We also thank George Rossman for infra-red data, and Pamela Champness, Ian Brough and Peter Kenway for their assitance with the electron microscopy at the Manchester Materials Science Centre (UMIST/Manchester University). The TEM work was supported by Daresbury Laboratory, Warrington, UK. We also acknowledge support from US National Science Foundation grant EAR-9118408.

References

Baur, W.H. (1981) Interatomic distance predictions for computer simulation of crystal structures. In *Structure and Bonding in Crystals II*, (A. Navrotsky and M. O'Keeffe, eds), Academic Press, New York, pp. 31–52.

Belakovskiy, D.I. (1991) Die seltenen Mineralien von Dara-i-Pioz im Hochgebirge Tadshikistans. *Lapis*, **16**(12), 42–8.

Brise, N.E. and O'Keeffe, M. (1991) Bond valence parameters for solids. *Acta Cryst.*, **B47**, 192–7.

Brown, I.D. and Altermatt, D. (1985) Bond valence parameters obtained from systematic analysis of the inorganic crystal structure database. *Acta Cryst.*, **B41**, 244–7.

Christy, A.G. (1995) Isosymmetric structural phase transitions: phenomenology and examples. *Acta Cryst.*, **B51**, 753–7.

Christy, A.G., Haines, J. and Clark, S.M. (1992) A Raman spectroscopic and energy-dispersive X-ray diffraction study of the high-pressure phase transitions of sodium hydrogen fluoride. *J. Phys. Condensed Matter*, **4**, 8131–40.

Grew, E.S., Belakovskiy, D.I., Fleet, M.E., Yates, M.G., McGee, J.J. and Marquez, N. (1993) Reedmergnerite and associated minerals from peralkaline pegmatite, Dara-i-Pioz, southern Tien Shan, Tajikistan. *Eur. J. Mineral.*, **5**, 971–84.

Grew, E.S., Yates, M.G., Belakovskiy, D.I., Rouse, R.C., Su, S.-C. and Marquez, N. (1994) Hyalotekite from reedmergnerite-bearing peralkaline pegmatite, Dara-i-Pioz, Tajikistan, and from Mn skarn, Långban, Värmland, Sweden: a new look at an old mineral. *Mineral. Mag.*, **58**, 285–97.

Haines, J. and Christy, A.G. (1992) Hydrogen bond formation in sodium and potassium hydrosulfides at high pressure. *Phys. Rev.*, **B46**, 8797–805.

Lindström, G. (1887) Om hyalotekit från Långban. *Öfversigt af Kongliga Vetenskaps-Akademiens Förhandlingar*, **9**, 589–93.

Moore, P.B., Araki, T. and Ghose, S. (1982) Hyalotekite, a complex lead borosilicate: its crystal structure and the lone-pair effect of Pb (II). *Amer. Mineral.*, **67**, 1012–20.

Moore, P.B., Sen Gupta, P.K. and Schlemper, E.O. (1985): Solid solution in plumbous potassium oxysilicate affected by interaction of a lone pair with bond pairs. *Nature*, **318**, 548.

Nordenskiöld, A. E. (1877) Nya mineralier från Långban. *Geologiska Föreningens i Stockholm Förhandlingar*, **3**, 376–84.

O'Keeffe, M. and Hyde, B.G. (1981) The role of non-bonded forces in crystals. In *Structure and Bonding in Crystals I*, (A. Navrotsky and M. O'Keeffe, eds), Academic Press, New York, pp. 227–54.

Peacor, D.R. and Buerger, M.J. (1962): Determination and refinement of the structure of narsarsukite, $Na_2TiOSi_4O_{10}$. *Amer. Mineral.*, **47**, 539–56.

Pring, A., Din, V.K., Jefferson, D.A. and Thomas, J.M. (1986) The crystal chemistry of rhodizite: a re-examination. *Mineral. Mag.*, **50**, 163–72.

Rouse, R.C. and Peacor, D.R. (1994) Maricopaite, an unusual lead calcium zeolite with an interrupted mordenite-like framework and intrachannel Pb_4 tetrahedral clusters. *Amer. Mineral.*, **79**, 175–84.

Scott, V. D. and Love, G. (1992) Formulation of a universal electron probe microanalysis correction method. *X-Ray Spectrum*, **21**, 27–35.

Taylor, W.H. and Náray-Szábo, St. (1931) The structure of apophyllite. *Z. Kristallogr.*, **77**, 146–58.

Watkin, D.J., Carruthers, P.W. and Betteridge, P.W. (1985) *CRYSTALS User Guide*. Chemical Crystallography Laboratory, University of Oxford.

[*Manuscript received 27 November 1996: revised 17 March 1997*]